

# A RIBBON OF TWINS FOR EXTRACTING VESSEL BOUNDARIES

B. Al-Diri\* and A. Hunter\*

\* The University of Lincoln

baldiri@lincoln.ac.uk

**Abstract:** This paper presents an efficient model for automatic detection and extraction of blood vessels in ocular fundus images. The model is formed using a combination of the concept of ribbon snakes and twin snakes. On each edge, the twin concept is introduced by using two snakes, one inside and one outside the boundary. The ribbon concept integrates the pair of twins on the two vessel edges into a single ribbon. The twins maintain the consistency of the vessel width, particularly on very blurred, thin and noisy vessels. The model exhibits excellent performance in extracting the boundaries of vessels, with improved robustness compared to alternative models in the presence of occlusion, poor contrast or noise. Results are presented which demonstrate the performance of the discussed edge extraction method, and show a significant improvement compared to classical snake formulations.

## Introduction

Vessel segmentation algorithms are a critical component of blood vessel analysis systems. The segmentation of vascular structures plays an important role in diagnosis, surgery and research, in many important systematic diseases such as diabetes and hypertension. Furthermore, the vascular tree seems to be the most appropriate representation for image registration applications.

A number of authors have investigated the use of active contour models in retinal vascular segmentation. However, none have reached the level of performance required for robust automatic detection of the entire network of blood vessels, which is needed for measurement techniques used for identifying and grading the severity of diabetic retinopathy. We have thus introduced a new parametric active contour model called a *ribbon of twins*. Our model uses the Gradient Vector Flow method – which provides good performance through concavities and noise features; the “twin” method – which uses two contours coupled by spring models to overcome initialization and localized feature problems; and the “ribbon” method, which couples two snakes with a consistent width parameter. Our model integrates these features to form a novel hybrid model.

## Parametric contours

In the parametric approach, an active contour [1] is represented as a curve or spline,  $v(s) = (x(s), y(s))$ , where

$v$  is a “vertex” and  $x$  and  $y$  represent the coordinates of the vertices and are functions of the normalised arc length  $0 \leq s \leq 1$ . The active contour has a dynamic behaviour that deforms from an initial position and hopefully converges to the boundary of the object. The energy functional  $E_{snake}^*$  composed of energy terms defines this behaviour:

$$E_{snake}^* = \int_0^1 E_{snake}(v(s)) ds \quad (1)$$

$$= \int_0^1 (E_{int}(v(s)) + E_{pho}(v(s)) + E_{ext}(v(s))) ds \quad (2)$$

– where  $E_{int}$  is the internal energy term that is based on the curve itself, which is designed to keep the model smooth during deformation;  $E_{pho}$  is the photometric energy term that arise from the image information, which is defined to move the model toward an object boundary or other desired feature within an image;  $E_{ext}$  is the external energy term that is proposed to improve the capture range of the photometric force.

## Internal energy

The internal energy consists of a first order term and a second order term [1].

$$E_{int} = \frac{\alpha(s)|v'(s)|^2 + \beta(s)|v''(s)|^2}{2} \quad (3)$$

where  $v'(s)$  and  $v''(s)$  denote the first and second derivative respectively, and parameters  $\alpha$  and  $\beta$  are the coefficients of the internal energy term and represent tension and rigidity, respectively.

## Photometric energy

The photometric energy is derived from the image to attract the snake toward desired objects such as boundaries. Given a grey-level image  $I(x, y)$ , the photometric energy leading an active contour towards edges is defined by [1]:

$$E_{pho}^{(1)} = -|\nabla I(x, y)|^2 \quad (4)$$

$$E_{pho}^{(2)} = -|\nabla(G_\sigma(x, y) * I(x, y))|^2 \quad (5)$$

where  $G_\sigma(x, y)$  is a two-dimensional gaussian filter with standard deviation  $\sigma$ ,  $\nabla$  is the gradient operator, and  $*$  is the 2D image convolution operator. The blurred gradient based approach has a number of limitations. First,

in boundary concavities the gradient vectors point in opposite directions and may cancel under smoothing [2]. Second, the algorithm has a limited capture range as the magnitude of the photometric force dies out quite rapidly away from the object boundary. Increasing  $\sigma$ , the smoothing filter size, increases this range but at the cost of less accurate and distinct boundary localization, ultimately obliterating concavities when  $\sigma$  becomes too large [2].

Alternative formulations have been suggested to overcome the limitations of the basic gradient formation.

Distance potential forces [3] were proposed to improve the capture range of the photometric force. In this approach, a thresholded edge map (a binary image) is generated. A potential function is computed using a Euclidean (or chamfer) distance map, which is based on the image information, and the negative gradient of this is used.

$$F_{ext} = -\nabla P(v) \quad (6)$$

The Euclidean distance map can be computed in different ways, for example [3]:

$$P(v) = -e^{d(v)^2} \quad (7)$$

where  $d(v)$  is the distance between a point  $v$  on the image and the nearest image edge pixel that is detected by an edge detector. The attraction potential force does not change the direction of the forces, only their magnitudes. Therefore, the problem of convergence to boundary concavities is not solved [2].

A more sophisticated approach is the Gradient Vector Flow (GVF) algorithm [2]; which provides a large capture range for the boundary, so the active contour does not have to be initialized close to the boundary. It also improves active convergence in concavities [4]. The GVF field is defined to be the vector field  $\mathbf{V}(x, y) = [\mathbf{u}(x, y), \mathbf{v}(x, y)]$  that minimises the energy functional ( $\epsilon$ ):

$$\epsilon = \int \int \mu(u_x^2 + u_y^2 + v_x^2 + v_y^2) + |\nabla f|^2 |\mathbf{V} - \nabla \mathbf{f}|^2 dx dy. \quad (8)$$

$$f(x, y) = -E_{pho}(x, y) \quad (9)$$

where  $f(x, y)$  is the photometric energy term that can be the gradient of the image, and  $\mu$  is a weighting parameter, also called a regularisation factor [2]. This is used to manage the trade off between the two terms of the integrand. When  $|\nabla f|$  is small (e.g. in homogeneous regions), the energy functional is dominated by the first term (smoothing term) yielding a slowly varying field. However, if  $|\nabla f|$  is large, the second term dominates the integrand, and the term is minimised when  $\mathbf{V} = \nabla \mathbf{f}$ . The choice of  $\mu$  depends on the amount of noise in the image – the more noise in the image, the larger  $\mu$  should be, since in the presence of noise the gradient increases and  $\mu$  should increase to control the trade off between the first and second terms in 8. However, GVF sometimes led to

edge delocalisation for boundary regions with low contrast and for boundary regions between nearby structure [5]. The parameter  $\mu$  should be as small as possible because as it increases edge delocalization gets worse.

### External energy

The External energy is used to provide high-level guidance to the active contour, to expedite convergence to the boundary and improve the capture range of the image force [6], and to compensate for problems such as a close-up of the Photometric force field within a boundary concavity. The most popular external energy terms are discussed below.

Springs and volcanoes were introduced by [1] as user-defined constraints that can be applied to an iterating active contour. A spring pulls the vertex toward itself with a force proportional to the distance between the spring point and the vertex:

$$E_{spring} = -k(p - v_i)^2 \quad (10)$$

where  $p$  and  $v$  are positions of the spring and the vertex, respectively, and  $k$  is a weighting factor. A volcano creates an expansive force that is applied to all vertices from a point  $c$  inside the region of interest. At each vertex this force is inversely proportional to the distance between point  $c$  and the vertex. A volcano is defined as:

$$E_{volcano} = \frac{1}{r^2} \quad (11)$$

where  $r$  is the distance between point  $c$  and the vertex.

A pressure force or balloon model [7] was proposed as an external force to improve the capture range of the gradient. The pressure force is independent of the image information and defines the direction of the active contour deformation by inflating or deflating it. Using this technique, the external force is composed of the Photometric and the pressure forces:

$$F_{ext} = k_{pressure} \mathbf{n}(s) - k \frac{\mathbf{F}_{phot}}{\|\mathbf{F}_{phot}\|} \quad (12)$$

where  $k_{pressure}$  is the pressure weighting and its positive or negative sign leads the active contour to inflate and deflate, respectively;  $\mathbf{n}(s)$  represents the unit vectors normal to vertices;  $k$  is the photometric force weighting where the photometric force is the gradient of the image.

The Dual Active Contour algorithm[8] was proposed as an external force (spring force) to overcome the primary problems of sensitivity to initialisation and undesirable convergence to insignificant localised or regionalised features [8]. An interior contour lies within the region of the desired feature and an exterior contour outside it. The two contours are coupled using springs which cause them to be attracted to each other in addition to suitable image features. The spring force is controlled by  $\lambda$ ,

$$E_{ext}(v(s)) = \lambda \frac{1}{2} (v(s) - \mathbf{mean}(s))^2 \quad (13)$$

where  $mean(s)$  is the mean contour of the interior and exterior contours.

$$\mathbf{mean}(s) = \frac{1}{2}(\mathbf{inner}(s) + \mathbf{outer}(s)) \quad (14)$$

The Dual snake includes a shape factor that forces the snake to adjust to a specific form (e.g., a circle).

The Central contour model and pressure contour model [9] were proposed to simplify the computational procedure. The central point model relies on the idea that motion of the contour points takes place along a predetermined number of fixed equally spacial radial lines which originate from an arbitrarily chosen contour centre point. The model tries to control forces on vertices with respect to the radial distance of snakes from the central point. Spatial co-ordinates of each contour snaxel can be computed from the following relationship:

$$\begin{aligned} x(s) &= x_0 + r(s)\sin\frac{2\pi s}{S_m} \\ y(s) &= y_0 + r(s)\cos\frac{2\pi s}{S_m} \end{aligned} \quad (15)$$

where  $x_0, y_0$  are the co-ordinates of the arbitrarily chosen contour central point,  $S_m$  is the number of contour snaxels,  $s$  is the snaxel number, i.e.  $s = 0, 1, \dots, S_m-1$  and  $r(s)$  is the radial distance of snaxel  $s$  from the central point. The pressure contour model aimed to extend active contour capabilities when the edges of complex shapes need to be extracted. The directions of the pressure forces have to be computed with high accuracy and the adjacent snaxels should not be too close to each other so that the computation of the perpendicular direction to the contour is based on a large contour fragment [9].

Sandwich snakes [10] [11] consists of two snakes looking for the same contour; for closed contours one snake is initially positioned inside the contour, and the other outside the contour; both snakes have equal number of particles, the corresponding particles are connected with a spring with an equilibrium length equal to zero. The energy function for sandwich snakes includes a new term in the internal energy; the coefficient  $\alpha$  is equal to zero to prevent the snake from minimizing its length [10]. The energy function of the sandwich snakes is:

$$\begin{aligned} E(p, q) &= \beta \sum_i | -p_{i-1} + 2p_i - p_{i+1} |^2 \\ &\quad + \beta \sum_i | -q_{i-1} + 2q_i - q_{i+1} |^2 \\ &\quad + \gamma \sum_i |p_i - q_i| - \lambda [|\nabla M(p_i)| + |\nabla M(q_i)|] \end{aligned} \quad (16)$$

where  $p_i$  denotes the position of the  $i^{th}$  particle for the internal snake, and  $q_i$  the position of the  $i^{th}$  particle for external snake.  $M(p_i)$  is the  $M$  image evaluated at the  $p_i$  position.

The twin snake algorithm [12] is an extension to the traditional snake, designed to detect two parallel contours simultaneously, and is useful for line extraction in high

resolution imagery. Lines in the image have two boundary contours close to each other; traditional snakes cannot guarantee to detect exactly one of the two, and in fact the extracted curve will jump between the two contours [12]. Therefore the twin snakes is used to find the two parallel contours simultaneously. The external attraction force is introduced as:

$$E_{ext}(v_i) = \delta_i(d_i - d_0)^2 \quad (17)$$

where  $\delta_i$  is a weight factor,  $d_i$  is the actual distance to the twin partner at point  $i$  and  $d_0$  the desired distance. The method often fails when using snakes for line extraction in high-resolution images [12]; unless the lines to be extracted can be defined as homogeneous, elongated areas with two parallel contours; also the depicted lines must have a width of at least three pixels, which guarantees that the two contours of the line can be detected independently [12]; this condition is not met in fine retinal vessels.

Ribbon snakes [13] [14], used for road extraction, extend the original snakes with a width component, defined as

$$\vec{v}(s, t) = (x(s, t), y(s, t), w(s, t)), (0 \leq s \leq 1) \quad (18)$$

where  $s$  is proportional to the length of the ribbon,  $t$  is the current time,  $x$  and  $y$  are the coordinates of the centerline of the ribbon, and  $w$  is the half width of the ribbon measured perpendicular to the centerline. For each slice of the ribbon  $\vec{v}(s_0, t_0)$  there exist two points  $\vec{v}_L(s_0, t_0)$  and  $\vec{v}_R(s_0, t_0)$  corresponding to the ribbons left and right sides. The position of these points which are composing the ribbons boundaries can be expressed as:

$$\begin{aligned} \vec{v}_R(s, t) &= w(s, t)\vec{n}(s, t) \\ \vec{v}_L(s, t) &= -w(s, t)\vec{n}(s, t) \end{aligned} \quad (19)$$

where  $\vec{n}(s, t)$  is the unit normal vector of the ribbon's centerline. The photometric term is:

$$p(\vec{v}(s, t)) = |\nabla I(\vec{v}_R(s, t))| + |\nabla I(\vec{v}_L(s, t))| \quad (20)$$

The function can be redefined [13] [14] as

$$p(\vec{v}(s, t)) = (\nabla I(\vec{v}_L(s, t)) - \nabla I(\vec{v}_R(s, t))) \cdot \vec{v}(s, t) \quad (21)$$

## Ribbon of Twins

We introduce a new parametric active contour model suitable for segmentation of retinal vessels and other fine, noisy, linear structures. Two twins of contours represent a ribbon along a vessel, with one twin on each edge of the vessel. Each twin consists of two contours, one inside and one outside the vessel. Each contour consists of a number of nodes. Corresponding nodes on the four contours are connected together to form a single integrated model. The two outside contours are connected by pull forces to the inside contours, while the inside contours are connected by push forces to each other; see Figure 1.

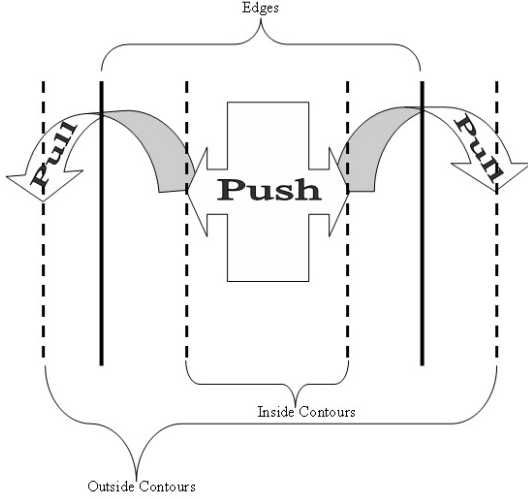


Figure 1: A Ribbon of Twin Diagram

The model is suitable for extracting vessels, roads or any tunnel shape. This model was tested on retinal vessels; we assumed that a segment of vessel has approximately parallel straight boundaries. We used the four contours to extract a segment-vessel boundary. The energy of four contours are defined as:

$$E_{contour}^{pos} = \int_0^1 \left( E_{int}^{pos}(v(s)) + E_{pho}^{pos}(v(s)) + E_{ext}^{pos}(v(s)) \right) ds \quad (22)$$

– where  $pos \in re, ri, le, li$  which refers to the position of the contours which are right external contour, right internal contour, left external contour and left internal contour. The internal energy is described in equation 3. The photometric energy is modified to

$$E_{pho} = -|GVF(f(x,y))|^2 \quad (23)$$

where  $f(x,y)$  is a photometric energy which is defined as

$$f(x,y) = G_{\sigma}(x,y) * I(x,y) \quad (24)$$

The external energy includes two different terms: the “push” and “pull” energies. The push energy is used inside the vessel to push contours toward interior boundary of the vessel and to maintain its width consistency, as described below:

$$E_{push} = -\frac{|VW - |v^r(n) - v^l(n)||^2}{2} \quad (25)$$

where  $VW$  is the vessel width,  $v^r(n)$  is the right contour,  $v^l(n)$  is the left contour, and  $n$  is the index of nodes. The vessel’s approximate width is calculated using one of the simple and traditional methods (e.g. [15],[16]).

The pull energy is used to pull the outside contours toward the inside contours, the pull energy is:

$$E_{pull} = -\frac{|v^i(n) - v^e(n)|^2}{2} \quad (26)$$

where  $i$  is internal contour and  $e$  is external contour.

The model converges when the maximum distance between two contours inside twins are less than a threshold ( $\theta$ ); the threshold is a sub-pixel value (e.g. 0.3 pixels). The edges of vessel are captured from both sides by inside and outside contours. The distance between the inside contours gives an extremely accurate estimated of the vessel width.

## Results

The ribbon snake has been previously used to extract roads and blood vessels. However, the performance on retinal vessels is not as good as on roads. This is due to the contrasting characteristics of roads and vessels. Roads have two parallel edges with a fixed width, in contrast to retina vessels. In addition, there are a lot of diseases that affect the vessels of the retina; causing changes in width, colour and the path of vessel. Adding to these difficulties, noise in retinal images often makes the vessel’s boundary blurred and fuzzy, particularly for vessels near the edge of the image.

We illustrate the performance of the new model on a number of typical problem cases found in retinal segmentation; the model parameters are GVF (iteration=90 and  $\mu = 0.02$ ),  $\sigma = 1.8$ , Twin-Threshold = 0.3;  $\beta =$  distance between two nodes which is equal 0.3 where  $\alpha$  is equal  $\beta/4$ .

The first case is performed on a noisy vessel segment, as shown in Figure 2.

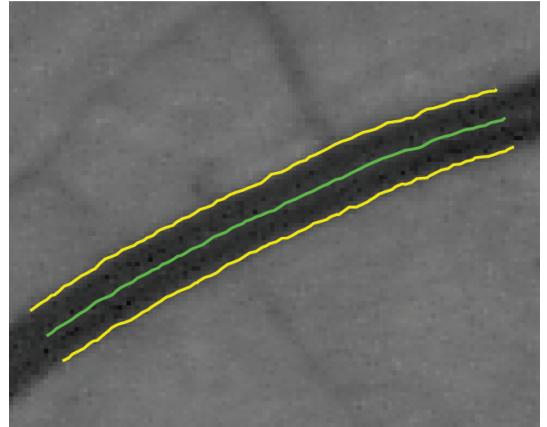


Figure 2: Convergence of the ribbon of twins on a single vessel with high noise around the vessel edges.

The second case shows the performance on very close vessels; their edges could be very blurred and the strong appearance edge of one vessel may affect the appearance edge of the other, particularly as the outside contours may initially be situated inside it’s neighbour vessel as in Figure 3. The outside contours will be pulled towards the inside contours; if the outside contours are stuck at any local minima where the local gradient force is greater or equal to the pull force and the maximum deformable distance of the outside contours is approximately zero, then the weight of the photometric term set to zero for next

iteration, allowing the outside contour to escape the local minimum.

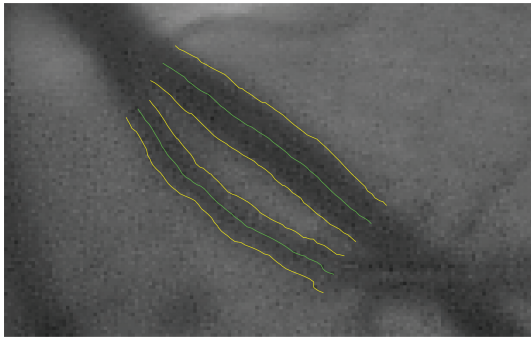


Figure 3: Two close vessel segments, where the contour converges correctly despite poor initializations.

The third case illustrates performance on a vessel which has a light reflex phenomenon; this causes significant problems for most vessel segmentation methods, making it difficult to calculate the width [17]. The proposed model is not affected by this phenomenon because the two inside contours are initiated far from the vessel centre, and the push-force push them outside toward edge, which has the opposite sense to any gradient forces related to the light reflex phenomenon, as in Figure 4.

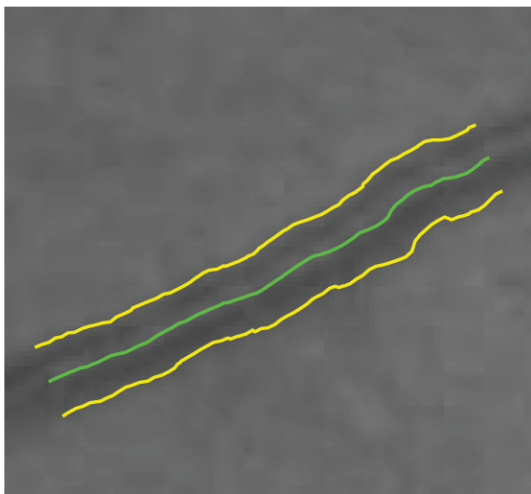


Figure 4: The model converges successfully on a vessel with a central light reflex.

The fourth case illustrates performance on very fine vessels. The majority of previously published methods fail to extract small vessels, which are important in diagnostic systems; the new model can extract and measure very tiny vessels, as shown in Figure 5.

The pull and push forces are normalized to keep the model balanced. Consequently the external forces are strongest at the initial stage, and weakest at the desired edge; these forces do not allow the contours to jump to the other side, as occurs in some snake formulations, because they pull the contours back.

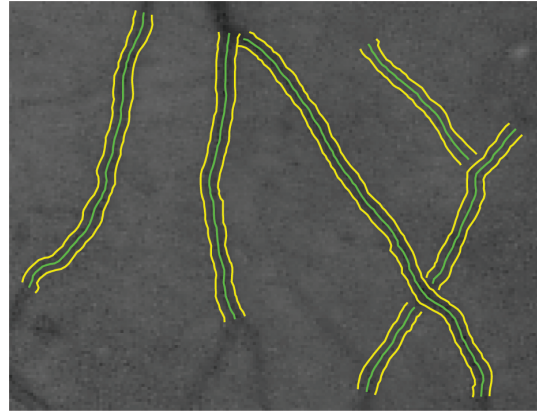


Figure 5: Convergence on very fine vessels.

## Conclusion

We have presented a new kind of snake called "a ribbon of twins". This consists of four contours to extract segments of vessel boundaries, a ribbon joining two twins. The model has robust behaviour, even with high levels of noise, and can accurately locate contours under difficult conditions, including: noisy blurred edges, closely parallel vessels, light reflex phenomenon, and very fine vessels. The model can extract tiny vessels which can not be extracted by alternative techniques. The model is more computationally expensive than the ribbon model, but the measurements are more accurate. The trade off between more computation and more accurate measurements and the previous models is governed by the purpose and usage of the model.

## References

- [1] KASS, M., WITKIN, A., TERZOPOULOS, D. (1988): 'Snakes: active contour models', *International Journal of Computer Vision*, **1(4)**, pp. 321-331
- [2] XU C. and PRINCE J. L. (1998): 'Snakes, Shapes, and Gradient Vector Flow', *IEEE Transactions on Image Processing*, **7(3)**, pp. 359-369
- [3] COHEN LD and COHEN I. (1993): 'Finite-element methods for active contour models and balloons for 2-D and 3-D images', *IEEE Trans. on PAMI*, **15 (11)**, pp. 1131-1147
- [4] HATAMZADEH-TABRIZI J. (2003): 'Using active contours for segmentation of middle-ear images', M. Eng. Thesis, McGill University, Montreal, Quebec.
- [5] HATAMZADEH-TABRIZI J. and FUNNELL WRJ (2002): 'Comparison of gradient, gradient vector flow and pressure force for image segmentation using active contours', *Proc 27th Ann Conf Can Med Biol Eng Soc (CD-ROM)*, 4 pp.
- [6] FENG Y. and GELENBE E. (1998): 'Adaptive object tracking and video compression with dynamic contours', *IEEE Proceedings of the Fifteenth Na-*

tional Radio Science Conf., NRSC, 1, INV3/1 - INV326.

- [7] COHEN LD, (1991): 'On active contour models and ballons', *CVGIP: Image Understanding*, **53(2)**, pp. 211-218
- [8] GUNN, S. R. and NIXON, M. S. (1994): 'A Model Based Dual Active Contour', In Proceedings of Proc. British Machine Vision Conference, 1994, pp. 305-314. Hancock, E., Eds.
- [9] SZCZYPINSKI P. and STRUMILLO P. (1996): 'Application of an Active Contour Model for Extraction of Fuzzy and Broken Image Edges', *Machine GRAPHICS and VISION*, **5(4)**, pp. 579-594
- [10] VELASCO FA. and MARROQUIN JL. (1998): 'Sandwich Snakes a robust parametric active contour', Proceedings of SPIE, San Diego Ca. USA, 1998, Image Analysis, Vol 3460, pp 226-236
- [11] VELASCO FA. and MARROQUIN JL. (2001): 'Robust parametric active contours: the Sandwich Snakes', *MACHINE VISION AND APPLICATIONS*, **12**, pp. 238-242
- [12] KERSCHNER M. (2000): 'Twin Snakes for Determining Seam Lines in Orthoimage Mosaicking', *International Archives of Photogrammetry and Remote Sensing*, **33**, Part B4, Amsterdam, pp. 454-461
- [13] BAUMGARTNER A., STEGER C., MAYER H., ECKSTEIN W., EBNER H. (1999): 'Automatic Road Extraction Based on Multi-Scale, Grouping, and Context', *Photogrammetric Engineering and Remote Sensing*, **65(7)**, pp. 777-786
- [14] LAPTEV I., MAYER H., LINDBERG T., ECKSTEIN W., STEGER C.T., BAUMGARTNER A. (2000): 'Automatic extraction of roads from aerial images based on scale space and snakes', *MVA*, **12(1)**, pp. 23-31
- [15] BRINCHMANN-HANSEN O., HEIER H. (1986): 'Theoretical relationships between light streak characteristics and optical properties of retinal vessels', *Acta Ophthalmolog. Suppl.*, **179**, pp. 33-37
- [16] GREGSON, P.H; et al, (2000): 'Automated Grading of Venous Beading', *Computers and Biomedical Research*, **28**, pp. 291-304
- [17] LOWELL J.A., HUNTER A., and STEEL D. (2002): 'Quantitative measurement of retinal vessel widths from fundus images based on 2d modelling', Tech. Rep. 06/02, Department of Computer Science, University of Durham, Science Labs., South Rd., Durham, UK, internet site address: <http://www.dur.ac.uk/computer.science/technicalreports/technical-reports.html>.